Rocznik Ochrona Środowiska

Volume 26 Year 2024 ISSN 2720-7501 pp. 728-744

https://doi.org/10.54740/ros.2024.064 open access

Received: August 2024 Accepted: December 2024 Published: December 2024

Enhanced Adsorption of Methylene Blue dye using Groundnut Shell Activated Nanocarbon: A Sustainable Approach

Muppidi Teja Gangadhar Reddy[1], Prabu Padanillay Chidambaram[2], Jothimani Palanisamy[3], Jeya Sundara Sharmila Devasahayam[4], Vijayakumary Ponnaian[5], Raja Kalimuthu[6], Pooluvapatty Murugan Shannmugam[7]*

[1]*Department of Environmental Sciences, Tamil Nadu Agricultural University, Coimbatore, Tamil Nadu, India*
https://orcid.org/0009-0007-1517-1856

[2]*Department of Environmental Sciences, Tamil Nadu Agricultural University, Coimbatore, Tamil Nadu, India*
https://orcid.org/0000-0002-7237-9481

[3]*Department of Environmental Sciences, Tamil Nadu Agricultural University, Coimbatore, Tamil Nadu, India*

[4]*Centre for Agricultural Nanotechnology, Tamil Nadu Agricultural University, Coimbatore, Tamil Nadu, India*
https://orcid.org/0000-0001-8865-0355

[5]*Department of Renewable Energy Engineering, Agricultural Engineering College and Research Institute, Tamil Nadu Agricultural University, Coimbatore, Tamil Nadu, India*
https://orcid.org/0000-0001-7933-8837

[6]*Centre for Agricultural Nanotechnology, Tamil Nadu Agricultural University, Coimbatore, Tamil Nadu, India*
https://orcid.org/0000-0003-2750-8085

[7]*Department of Agronomy, Tamil Nadu Agricultural University, Coimbatore, Tamil Nadu, India*
https://orcid.org/0000-0002-6706-8419

[*]*corresponding author's e-mail: prabu.pc@tnau.ac.in*

Abstract: In this work, activated nanocarbon derived from lignocellulose-rich groundnut shells was synthesized by KOH impregnation to enhance surface area and porosity, resulting in Groundnut Shell Activated Nanocarbon (GSANC) and thoroughly characterized for its porosity, particle size, crystallinity, combustion profile, functional groups, and surface morphology. It exhibited a type I N_2 adsorption-desorption isotherm with an H4 hysteresis loop, indicative of a mix of micro and mesopores, with a high specific surface area of 665.80 $m^2\ g^{-1}$ and an average pore diameter of 2.97 nm. This nanoparticulate activated carbon exhibited exceptional performance in methylene blue (MB) dye adsorption, achieving a maximum adsorption capacity (q_{max}) of 212.76 mg g^{-1}. The adsorption mechanisms included electrostatic interactions, π-π stacking, and hydrogen bonding, contributing significantly to its efficacy as an adsorbent highlighting its potential for applications in wastewater treatment.

Keywords: groundnut shell, activated carbon, KOH, methylene blue, adsorption

1. Introduction

Organic dyes are compounds that impart colour to materials and are categorized based on their chemical structures, including azo dyes, anthraquinone dyes, and phenothiazine dyes (Benkhaya et al. 2022, Hashemi & Kaykhaii 2022). The synthetic basic dye Methylene Blue (MB) belongs to the phenothiazine group, with the chemical formula $C_{16}H_{18}ClN_3S$ (Eldeeb et al. 2024, Salimi & Roosta 2019). It is a cationic dye with a positive charge, widely used in industries like textiles, leather, paper, and plastics, and causes significant environmental challenges due to its visibility and toxicity even at low concentrations (Sen 2023). Because of its high reactivity and adsorption capability, activated carbon is a highly effective method for removing MB dye from wastewater. However, the cost of activated carbon is a significant drawback. To mitigate this, efforts have been made to produce activated carbon from agricultural wastes containing lignocellulosic compounds, which exhibit properties akin to nanomaterials, offering a more cost-effective and sustainable solution having great potential for removal of different pollutants like dyes (Sawalha et al. 2022, Supong et al. 2019, Tsade Kara et al. 2021). These could be low-cost, eco-friendly, regenerative, and abundant (Zhou et al. 2015). Groundnut shells are rich in lignocellulosic polymer materials, giving them significant potential as a precursor for biochar and activated carbon production (Al-Othman et al. 2012). Activated nanocarbon made from groundnut shells has a high surface area, porous structure, pore diameter, and cation exchange capacity, making it an excellent material for adsorption (Shan et al. 2020). Even though the activation of biomass can be done by different activation methods physically and chemically, KOH is regarded as an effective activator when producing activated carbon with a predominantly microporous structure (Nam et al. 2018). The present study aimed to synthesis, characterize and evaluate the efficiency of groundnut shell activated nano carbon on methylene blue adsorption.

2. Experimental Work

2.1. Materials

Groundnut shells are collected from the Department of Oil Seeds, Tamil Nadu Agricultural University, Coimbatore, India. KOH is procured from Himedia Laboratories Pvt. ltd., Mumbai, India. Methylene blue was purchased from Isochem Laboratories, Kochi, India.

2.2. Preparation of groundnut shell biochar and activated nanocarbon

Groundnut shells are washed with deionized water and dried in the hot air oven. After drying, shells are pulverized, sieved through a 100-mesh sieve, and stored in a place with less moisture. The pulverized shells are pyrolyzed to pristine biochar at 500°C in a pyrolysis unit under a limited atmosphere. After washing with distilled water, the biochar was dried in a hot air oven at 80°C for 24 hours. This procedure produced pristine Groundnut Shell Biochar (GSBC). A weight of 6.0 g GSBC was loaded in centrifuge tubes, mixed with 6.0 g KOH and 20 mL distilled water, and oscillated on a shaker for 24 hours. The biochar was then dried at 80°C for 24 hours, placed in a ceramic crucible, and activated at 700°C for 2 hours in a muffle furnace with a heating rate of 5°C min^{-1}. After cooling, 5 g of the modified biochar was mixed with 10 mL of 10% H_2SO_4 and oscillated for 2 hours to create exfoliated biochar with nanocarbon properties. The product was washed with deionized water and 0.1M HCl until neutral pH, then dried at 80°C for 24 hours. The resulting nanocarbon is called Groundnut Shell Activated Nano Carbon (GSANC) and stored in an inert, low-moisture environment.

2.3. Physio-chemical characterization studies

For surface morphology, GSBC and GSANC were analyzed using FESEM with EDS (Tescan - Mira3 XMU, Czech Republic) to analyse the physio-chemical characteristics. BET surface area analysis (Quantachrome® ASiQwinTM, United States of America) was used for specific surface area measurements. XRD (Shimadzu 6000, Japan) identified mineral composition, and FTIR (Shimadzu, Japan) detected reactive functional groups. TGA/DTG (EXSTAR/G300) to determine the combustion profile of the materials. Ultimate analysis of raw groundnut shell, groundnut shell biochar, and groundnut shell nano carbon was performed with a CHNS-O analyzer (Thermo Finnigan FLASH EA 1112 Series, United States of America).

2.4. Adsorption studies of MB on GSANC

The adsorption efficiency of GNANC on MB was optimized by varying the GSANC dosage (0.02-0.10 g), initial MB concentrations prepared from the stock solution, diluted to (10-50 mg L^{-1}), and solution pH (2-12). 100 mL MB solution in 250 mL Erlenmeyer flasks were stirred at 100 strokes min^{-1} in a water bath shaker. Absorbances at 661 nm were measured using a HACH DR 2800 UV-vis spectrophotometer, and concentrations were determined from a calibration curve. The equilibrium isotherm was determined at 303 K with initial MB concentrations of 10-50 mg L^{-1} and contact times of 0-360 minutes. The percentage of dye removal (DR %) and adsorption capacity (q_e) were calculated by Equations (1) and (2), respectively.

$$DR\ \% = \frac{(C_o - C_e)}{C_o} \times 100 \tag{1}$$

$$q_e = \frac{(C_o - C_e)V}{W} \tag{2}$$

where:
C_o (mg L^{-1}) – Initial concentration of MB dye,
C_e (mg L^{-1}) – Equilibrium concentrations of MB dye,
q_e (mg g^{-1}) – Amount of dye adsorbed at equilibrium,
V (L) – Volume of dye solution,
W (g) – GSANC dosage.

3. Results and Discussion

3.1. Characterization of GSBC and GSANC

3.1.1. FESEM with EDS

Figure 1 shows the FESEM micrographs used to compare the morphological structures of GSBC (a & b) and GSANC (c & d). Initially, the biochar surface is uneven, but it has a smooth texture. After activation with KOH and treatment with 10% H_2SO_4, the biochar shows distinct porous features and layered structures, enhancing the formation of micropores and mesopores. This increases the surface-active sites, improving the adsorption capacity for metal ions and organic pollutants. Elemental composition via EDS spectra for GSBC (Figure 2) and GSANC (Figure 3) is in Table 1. KOH is more effective than other chemical agents due to its ability to form intercalation compounds with carbon. The activation process involves carbon gasification, CO_2 release, and the reduction of K_2O to K, leading to pore development explained in the equations (3) to (10) given below (Wang et al. 2016, Xu et al. 2019).

$$2KOH \rightarrow K_2O + H_2O \quad (3)$$

$$H_2O + C \rightarrow CO + H_2\uparrow \quad (4)$$

$$CO + H_2O \rightarrow CO_2 + H_2\uparrow \quad (5)$$

$$CO_2 + K_2O \rightarrow K_2CO_3 \quad (6)$$

$$K_2CO_3 \rightarrow K_2O + CO_2 \quad (7)$$

$$CO_2 + C \rightarrow 2CO \quad (8)$$

$$K_2O + 2C \rightarrow K + 2CO\uparrow \quad (9)$$

$$K_2CO_3 + C \rightarrow 2K + 3CO\uparrow \quad (10)$$

The activation of carbon with KOH occurs in three stages. In the primary stage, H_2O and CO_2 formation (eq. 3-5) develop porosity in the carbon. Later temperatures near and above 700°C, K_2O and K_2CO_3 formation (eq. 6-8) etches the carbon structure, creating a porous framework through redox reactions. Above 700°C, metallic potassium formation (eq. 9 and 10) is crucial for developing porosity by incorporating and diffusing potassium into the carbon's internal structure, creating new pores and expanding existing ones in the final stage.

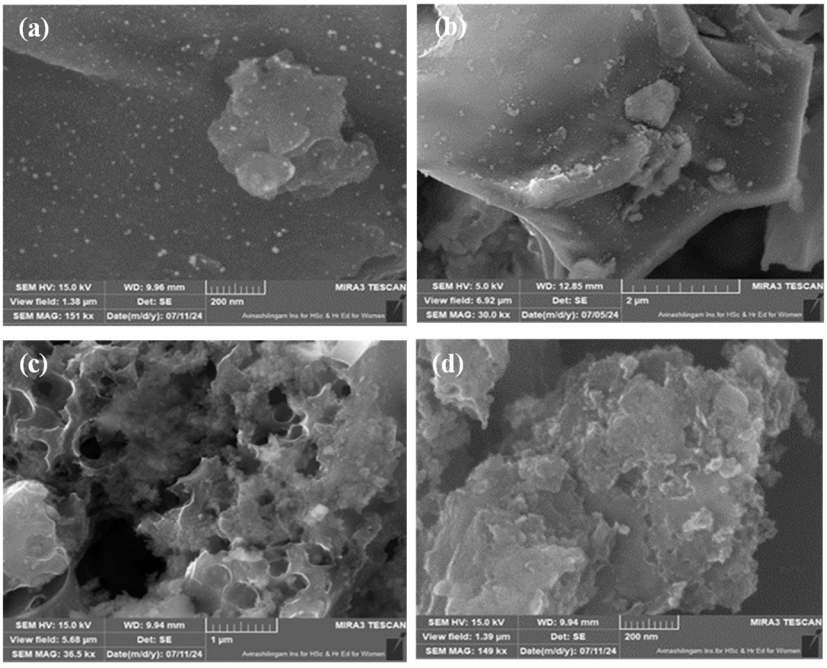

Fig. 1. FESEM micrographs of GSBC (a) 200 nm, (b) 2 µm, and GSANC (c) 1 µm, (d) 200 nm

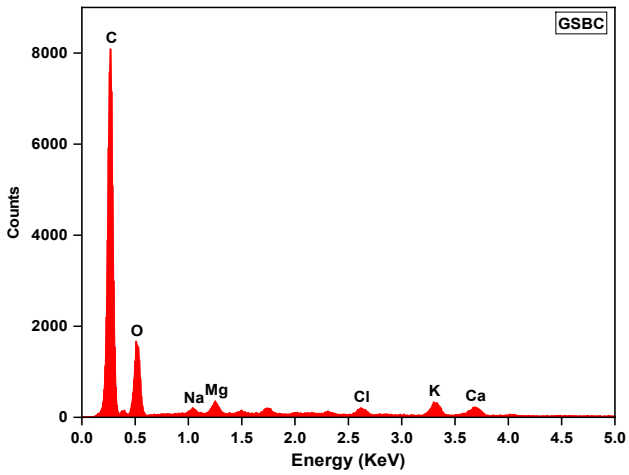

Fig. 2. EDS spectra of GSBC

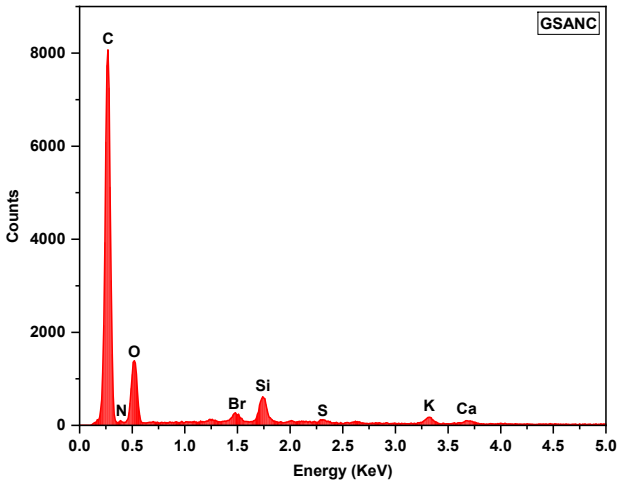

Fig. 3. EDS spectra of GSANC

Table 1. EDS spectral composition of GSBC and GSANC

Samples		Chemical composition										
		C K	O K	N K	Si K	Br L	K K	Ca K	S K	Cl K	Mg K	Na K
GSBC	Weight %	61.15	27.00	-	-	-	3.83	3.26	-	1.45	1.80	1.51
GSANC	Weight %	66.20	23.93	1.26	3.00	1.77	1.80	1.28	0.77	-	-	-

3.1.2. BET Surface area analysis

Bruneuer-Emmett-Teller surface area analysis shows a substantial rise in the surface area of GSANC compared to GSBC. High-temperature KOH impregnation increases the surface area and total pore volume by creating porous activated carbon through interactions with gasification. The N_2 adsorption-desorption isotherm plots for GSBC and GSANC are shown in Figures 4 and 5, respectively, with textural properties in Table 2. Figure 4 shows GSBC with a rare Type III isotherm, lacking limiting adsorption at high relative pressure (p/p_o). Figure 5 shows GSANC with a Type I isotherm and a Type IV (H4) hysteresis loop (Sing 1985). Due to micropore filling, GSANC displays a sharp rise in adsorption at low relative pressure. At greater pressure, however, multilayer adsorption and capillary condensation are seen, signifying the presence of both micropores and mesopores. Capillary condensation at P/P_o above 0.4 suggests broad slit-like mesopores in GSANC. BET analysis reveals that the GSANC has a specific surface area of 665.80 $m^2\ g^{-1}$, a total pore volume of 0.495 $cm^3\ g^{-1}$, and an average pore diameter of 2.97 nm. Micropores contribute 612.28 $m^2\ g^{-1}$ (91.96%) of the surface area.

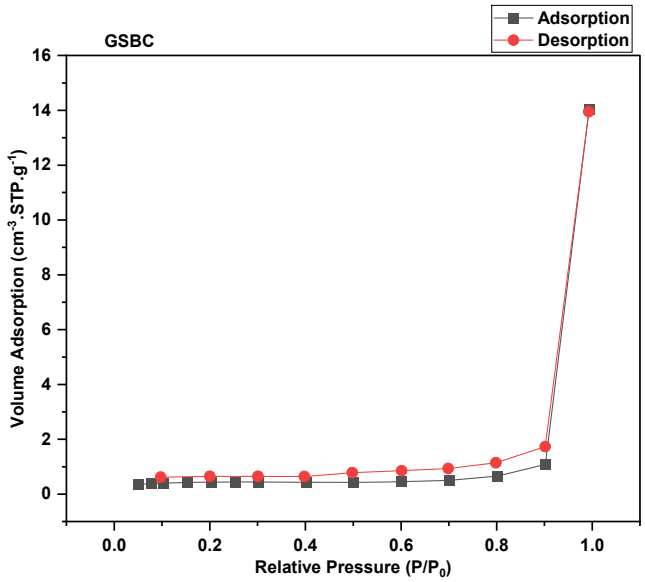

Fig. 4. N_2 adsorption-desorption isotherms of GSBC

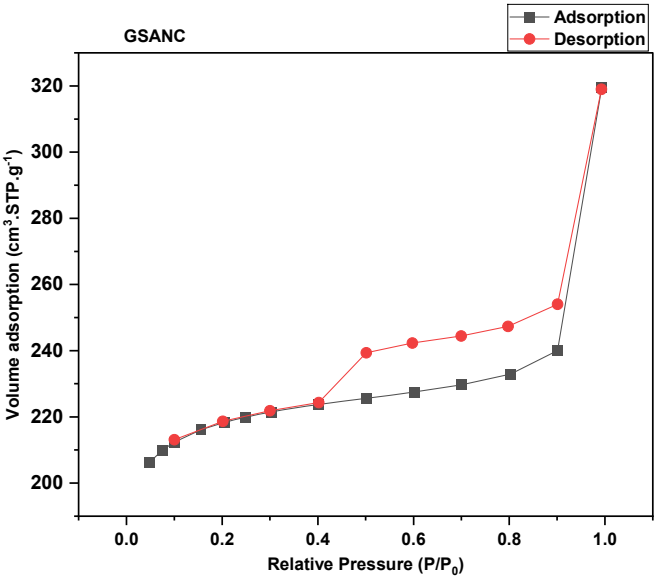

Fig. 5. N_2 adsorption-desorption isotherms of GSANC

Table 2. Textural properties of GSBC and GSANC

Properties	Units	Samples	
		GSBC	GSANC
S_{BET}	$m^2\ g^{-1}$	1.36	665.80
$S_{Langmuir}$	$m^2\ g^{-1}$	0	1464.31
S_{BJH}	$m^2\ g^{-1}$	1.32	103.42
S_{Ext}	$m^2\ g^{-1}$	0.07	53.51
S_{mi}	$m^2\ g^{-1}$	1.43	612.28
V_t	$cm^3\ g^{-1}$	0.21	0.49
V_{mi}	$cm^3\ g^{-1}$	0.001	0.31
Average pore size	nm	6.39	2.97
V_{BJH}	$cm^3\ g^{-1}$	0.02	0.19
W_{BJH}	nm	3.62	3.65
Particle size	nm	1034	118

3.1.3. XRD analysis

The XRD pattern depicted in Figure 6 reveals that GSBC exhibits a broad peak near 23° along with distinct sharp peaks, suggesting both crystallinity and the presence of a small quantity of other minerals (Shan et al. 2020). In contrast, GSANC has distinct peaks at 2θ values of about 23° and 44°, corresponding to the (002) and (100) planes of graphitic crystallites, with broad peaks suggesting an amorphous nature.

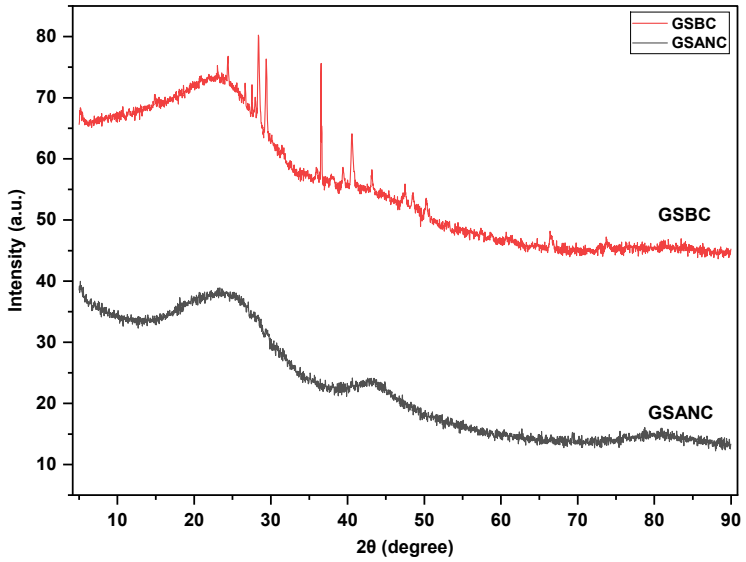

Fig. 6. XRD patterns of GSBC and GSANC

3.1.4. TGA/DTG analysis

The TGA/DTG analysis of GSBC (Figure 7) and GSANC (Figure 8) revealed a distinct three-step weight loss. The first stage, occurring between 20-200°C, indicated a significant weight reduction corresponding to the removal of moisture from the sample. The second stage, between 200-500°C, showed a substantial weight loss attributed to pyrolysis or carbonization, as volatiles and tar substances were eliminated. In the third stage, during the temperature range of 500-700°C, the breakdown of a high-strength structure was observed (Inyang et al. 2012). Beyond 700°C, the weight loss was minimal, indicating the stability of the adsorbent's basic structure.

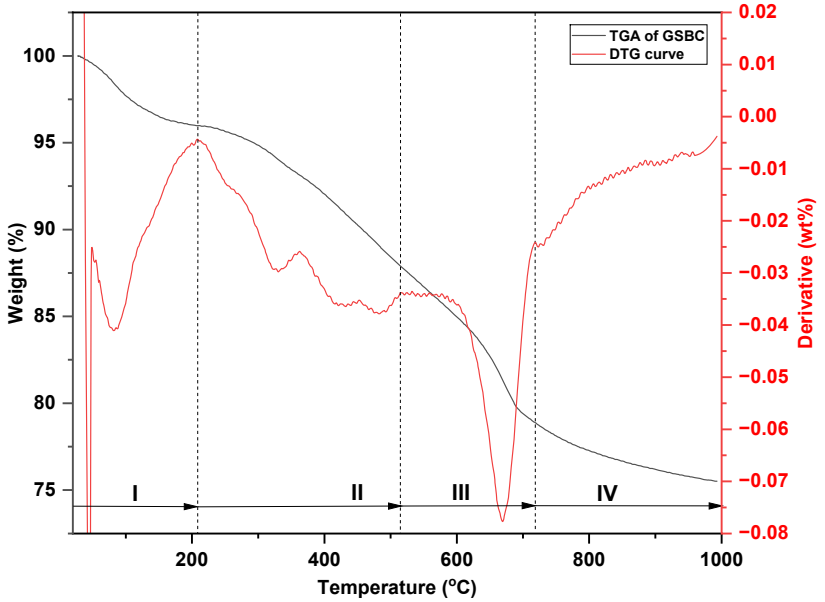

Fig. 7. TGA/DTG results of GSBC

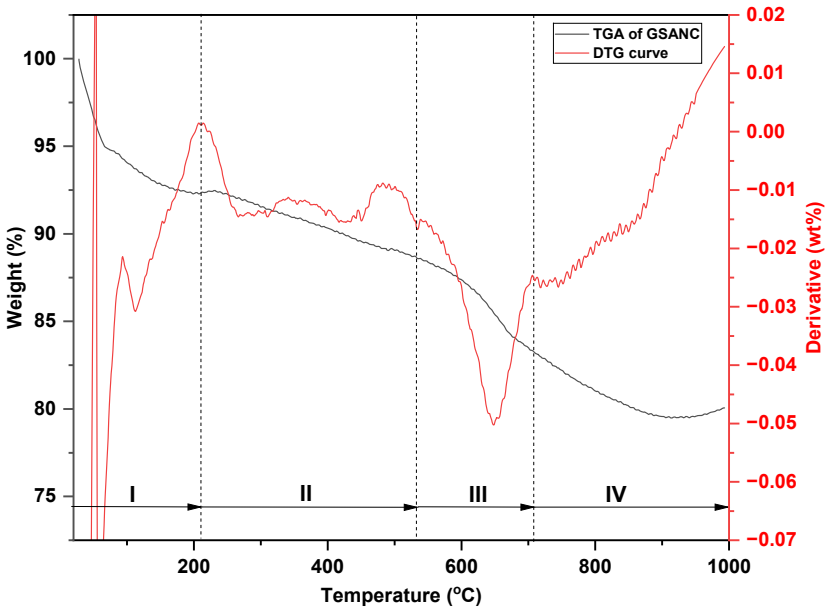

Fig. 8. TGA/DTG results of GSANC

3.1.5. FTIR analysis

The functional groups detected by FTIR analysis (Figure 9) show the following for GSBC: absorption at 1553.488 cm^{-1} (N-O stretching), 1397.537 cm^{-1} (C-O stretching), 689.192 cm^{-1} (C=C bending), and 511.901 cm^{-1} (C-Cl stretching). For GSANC (Figure 10), absorption at 3819.699 cm^{-1} (OH stretch), 3628.454 cm^{-1} (alcoholic OH stretch) (Lian et al. 2011, Xing et al. 2008), 3090.834 cm^{-1} (=C-H stretch), 2326.675 cm^{-1} (C=N nitrile stretch), 1505.882 cm^{-1} (C=O amide stretch) (Georgin et al., 2016), and 713.816 cm^{-1} (C=C bending) (Uchimiya et al. 2011).

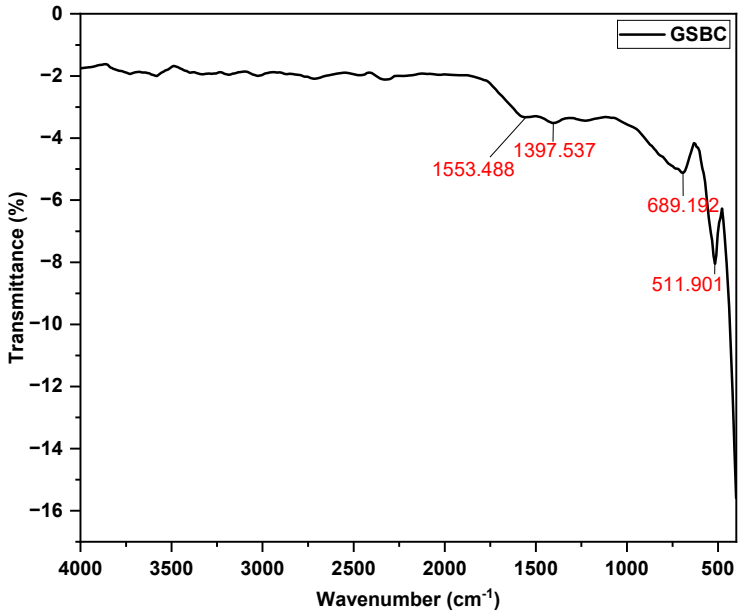

Fig. 9. FTIR spectra of GSBC

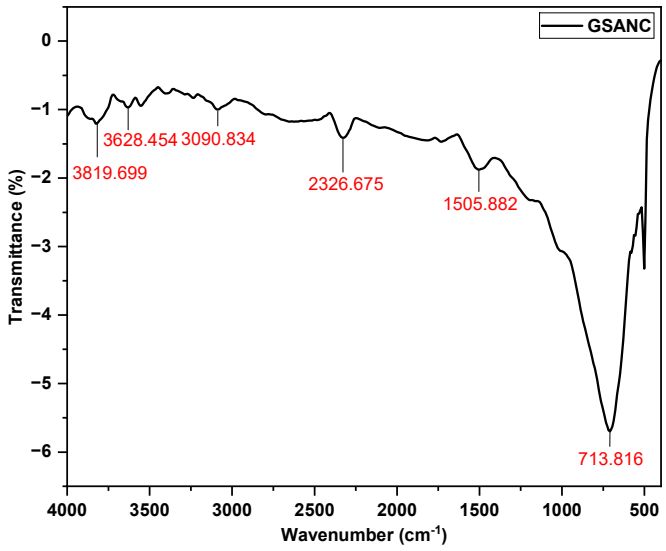

Fig. 10. FTIR spectra of GSANC

Table 3. Chemical characterization of raw groundnut shells, GSBC and GSANC

Sample	Groundnut shells	GSBC	GSANC
Chemical constituents (%)			
Cellulose	37.138	-	-
Hemicellulose	15.78	-	-
Lignin	30.58	-	-
Proximate analysis (%)			
Moisture content	0.7	1.06	3.02
Volatile matter	52.32	42.21	34.67
Fixed carbon[a]	18.34	41.127	56.03
Ash content	29.34	16.663	9.300
Ultimate analysis (%)			
C	41.670	67.814	71.733
H	5.790	1.972	3.604
N	1.438	0.856	0.484
S	1.090	0	0
O[b]	20.672	12.695	14.879

[a]Presented in terms of dry basis
[b]Estimated by the difference: O% = 100 - C - H - N - S – ash

From Table 3, the ultimate analysis states that the H/C molar ratio indicator of the degree of aromaticity and stability of GSBC and GSANC was calculated at 0.02 and 0.05, respectively, falling below the threshold of 0.7, aligning with the standards set by the International Biochar Initiative (IBI 2015) and EU guidelines (EBC 2012). Similarly, the O/C molar ratio indicates the oxidation level and the extent of carbonization of GSBC and GSANC was 0.18 and 0.208, meeting the EU guidelines' requirement of being below 0.4.

3.2. Adsorption studies

3.2.1. Effect of GSANC dosage

The effect of GSANC dosage on the removal of MB dye was investigated by varying the adsorbent amount to 0.02-0.10 g, while maintaining all other parameters constant, as shown in Figure 11. The efficiency of MB dye removal increased significantly by 24.2-99.9% as the adsorbent dosage was increased by 0.02-0.08 g.

It was clear that increasing the adsorbent dose to more than 0.08 g cannot show any significant dye removal. Since the maximum removal of MB dye ions of 99.9% was achieved with a 0.08 g dosage, this amount of GSANC was selected for future applications.

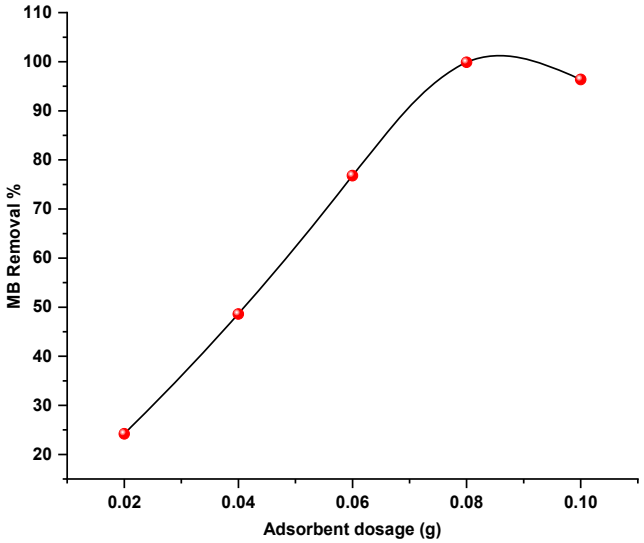

Fig. 11. Effect of adsorbent dosage on MB removal %

3.2.2. Influence of pH

The pH of a solution significantly affects the adsorption process by modifying the adsorbent's surface charge and the adsorbate molecules' ionization degree. To investigate the effect of pH on the removal of MB dye ions, experiments were carried out across a pH range of 2-12 using an optimized dosage of GSANC, while keeping other parameters constant (30 mg L^{-1} concentration, 0.08 g adsorbent dosage, 360 minutes contact time). Understanding MB dye uptake at various pH levels requires identifying the point where the adsorbent's surface has a neutral net charge, known as the point of zero charge (pH_{zpc}). The pKa value of MB dye, which is 3.8 (Eldeeb et al. 2024), indicates that MB dye molecules exist in cationic form in the solution. The pH_{zpc} of GSANC is slightly basic at 7.2. The highest adsorption capacity of 45.35 mg g^{-1} was observed at pH 8 (Figure 12), a basic condition where the GSANC surface acquires a negative charge, thereby attracting MB molecules through electrostatic attraction. At the lowest pH values of the adsorbent, repulsive electrostatic attraction forces between MB dye ions and positively charged functional groups of GSANC adsorbent (Tsade Kara et al. 2021). At the alkaline pH of the solution, the adsorbent becomes negatively charged, which leads to the effective removal of cationic MB dye ions. Consequently, pH 8 is adopted as the optimized pH solution for further experiments.

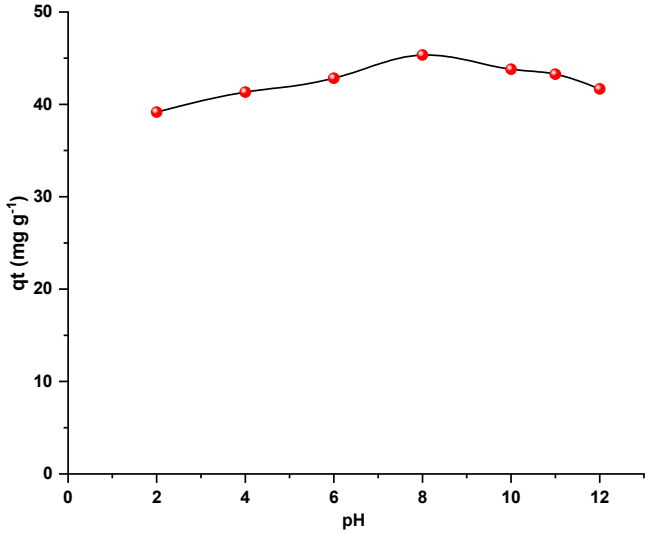

Fig. 12. Effect of pH on adsorption capacity

3.2.3. Effect of the initial concentration and contact time

The effects of contact time and initial concentrations of MB dye (ranging 10-50 mg L^{-1}) on the adsorption capacity of GSANC were evaluated using optimized parameters. The adsorption capacities of GSANC at a specific time, denoted as q_t (mg g^{-1}), were plotted against time (minutes) for various MB dye concentrations, as illustrated in Figure 13. The adsorption capacity of GSANC was observed to increase 12.48-45.35 mg g^{-1} as the concentration of MB dye rose 10-50 mg L^{-1}. In the early stages of the process, there was a swift increase in adsorption capacity at all concentrations, likely due to the abundance of available adsorption sites on the GSANC for MB dye uptake. As the process progressed, the adsorption rate gradually declined and eventually stabilized, signalling that equilibrium between the adsorbent and the adsorbate was being reached. Equilibrium times for the GSANC-MB interaction were achieved at 210, 270, 300, 330, and 330 minutes for concentrations of 10, 20, 30, 40, and 50 mg L^{-1}, respectively. At higher MB dye concentrations, more time was needed to achieve equilibrium due to the concentration gradient, which facilitates the diffusion of dye into the internal pores and surface of the adsorbent.

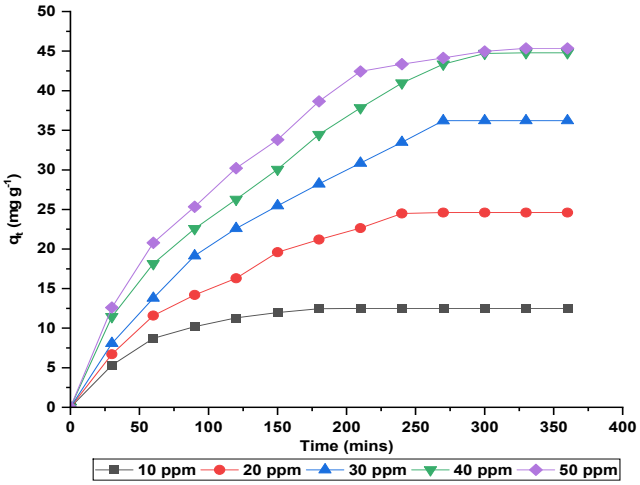

Fig. 13. Effect of the contact time on MB dye adsorption at different initial concentrations

3.2.4. Adsorption kinetics and modelling

Understanding the kinetics and identifying the rate-determining step is essential to design an effective adsorption system. In this study, three kinetic models, pseudo-first order (PFO) (Lagergren 1898), pseudo-second order (PSO) (Ho & McKay 1999), and Elovich (Senthilkumaar et al. 2005), were applied to the experimental data to elucidate the adsorption mechanism of methylene blue (MB) dye on GSANC. Linear forms of these models were used to minimize statistical bias. The best fitted model was selected based on the highest coefficient of determination (R^2) from the respective equations for PFO (eq. 11), PSO (eq. 12), and Elovich (eqs. 13a and 13b).

$$\log (q_e - q_t) = \log q_e - \frac{k_1}{2.303} t \tag{11}$$

$$\frac{t}{q_1} = \frac{1}{k_2 qe^2} + \frac{t}{q_e} \tag{12}$$

$$\frac{dq_t}{d_t} = \alpha e - \beta q_t \tag{13a}$$

(or)

$$q_t = q_o + \frac{1}{\beta}\ln(\alpha\beta) + \frac{1}{\beta}\ln(t) \tag{13b}$$

where:
k_1 (min^{-1}) – Lagergren's PFO kinetic parameter,
q_t (mg g^{-1}) – Amount of dye adsorbed at time t,
q_e (mg g^{-1}) – Amount of dye adsorbed at equilibrium,
k_2 (g mg^{-1} min^{-1}) – PSO kinetic parameter,
α (mg g^{-1} min^{-1}) – Initial adsorption rate,
β (g mg^{-1}) – Extent of surface coverage and the activation energy for chemisorption.

Using an initial concentration (C_o) of 30 mg L^{-1}, Figures 14, 15 and 16 illustrate the PFO, PSO, and Elovich model plots, while Table 4. presents the extracted parameters and their R^2 values. The analysis shows that MB adsorption by GSANC follows the PSO model, as indicated by higher R^2 values.

Table 4. PFO, PSO and Elovich kinetic parameters for MB dye adsorption by GSANC

	PFO			PSO			Elovich		
C_o (mg L^{-1})	q_e cal (mg g^{-1})	k_1 (mg g^{-1} min^{-1})	R^2	q_e cal (mg g^{-1})	k_2 (mg g^{-1} min^{-1})	R^2	α	β	R^2
10	4.45	0.004	0.43	13.47	0.003	0.99	1.86	0.42	0.95
20	5.23	0.005	0.56	30.21	0.0004	0.94	2.02	0.21	0.87
30	6.01	0.006	0.53	47.39	0.0001	0.90	2.46	0.14	0.83
40	7.17	0.006	0.56	57.14	0.0001	0.90	3.09	-2.1	0.84
50	8.05	0.006	0.51	58.24	0.0002	0.94	3.65	-2.1	0.87

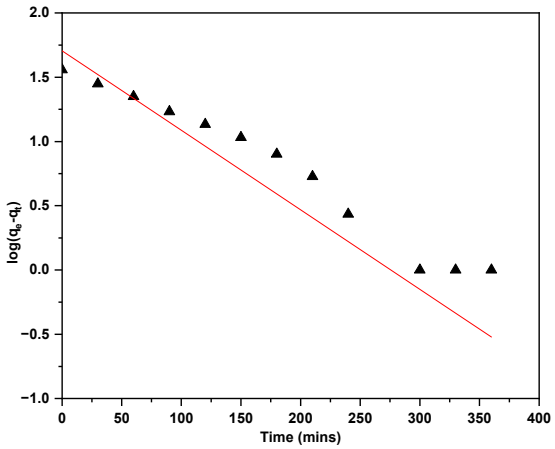

Fig. 14. PFO model for MB dye adsorption by GSANC

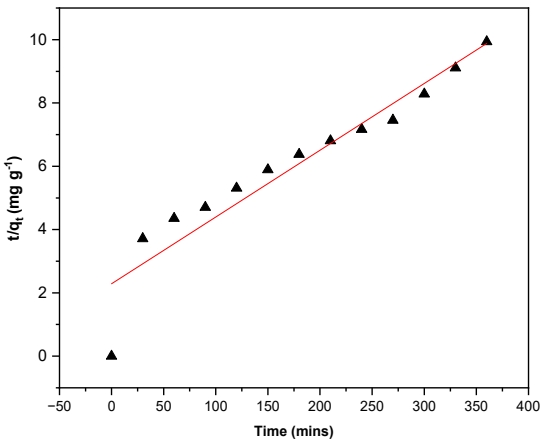

Fig. 15. PSO model for MB dye adsorption by GSANC

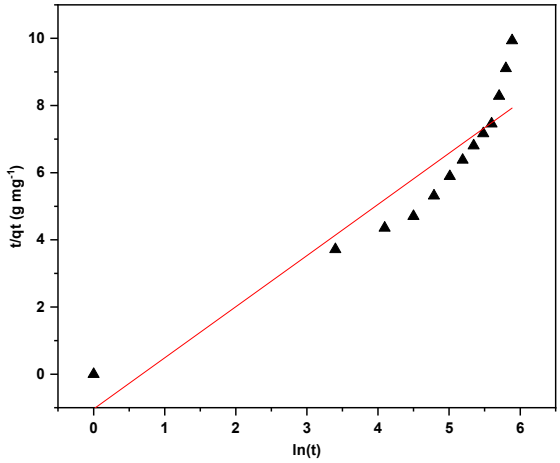

Fig. 16. Elovich model for MB dye adsorption by GSANC

3.2.5. Isotherm modelling

The adsorption capacities of GSANC were evaluated at initial concentrations of 30, 40, and 50 mg L^{-1}. The interaction between MB dye and GSANC was analyzed using Langmuir (Langmuir 1916), Freundlich (Bulut & Aydın 2006), and Temkin isotherm (Temkin & Pyzhev 1940) models. The Langmuir model (eq. 14a) describes monolayer adsorption on fixed sites, with the Langmuir constant R_L given in eq. 14b. The Freundlich model (eq. 15) describes multilayer adsorption on heterogeneous surfaces. The Temkin model (eq. 16) accounts for decreased adsorption heat with increased coverage, reflecting adsorbent-adsorbate interactions.

$$\frac{C_e}{q_e} = \frac{1}{K_L X_m} + \frac{C_e}{X_m} \tag{14a}$$

$$R_L = \frac{1}{1 + K_L . C_o} \tag{14b}$$

$$\log q_e = \log K_F + \frac{1}{n} \log c_e \tag{15}$$

$$q_e = \frac{RT}{B} \ln K_T + \frac{RT}{B} \ln C_e \tag{16}$$

where:
q_e (mg g^{-1}) – Amount of dye adsorbed at equilibrium,
C_e (mg L^{-1}) – Equilibrium dye concentration,
X_m (mg g^{-1}) – Maximum adsorption capacity,
K_L – Langmuir constant,
C_o – Initial concentration,
K_F and n – Freundlich constants,
B (J mol^{-1}) – Temkin constant,
k_T (L g^{-1}) – Temkin isotherm energy constant,
b_T (J mol^{-1}) – Heat of adsorption,
R – Gas constant (8.314 J mol^{-1} K).

Based on R^2 values from the isotherm models in Table 5, the adsorption of MB onto the GSANC surface was analyzed. Figures 17, 18, and 19 illustrate the Langmuir, Freundlich, and Temkin isotherms for MB dye adsorption by GSANC, with a constant adsorbent dosage of 0.08 g, solution pH of 8, temperature set at 30°C (303 K), an agitation speed of 150 strokes, and a 100 mL volume of MB solution.

Table 5. Parameters of isotherm models for MB dye adsorption by GSANC at 30°C.

Adsorption isotherm	Langmuir			Freundlich			Temkin		
Parameter	q_{max} (mg g^{-1})	K_L	R^2	K_F (mg g^{-1}) (L mg^{-1})1/n	n	R^2	K_T (L mg^{-1})	b_T (J mol^{-1})	R^2
Value	212.76	0.21	0.99	1.22	0.63	0.82	0.69	199	0.99

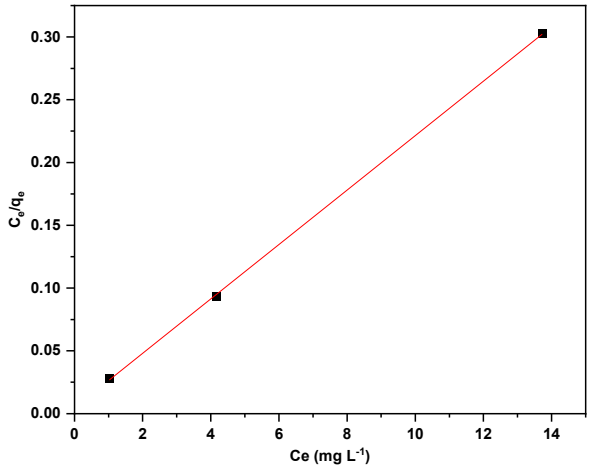

Fig. 17. Langmuir adsorption isotherm of MB dye adsorption by GSANC

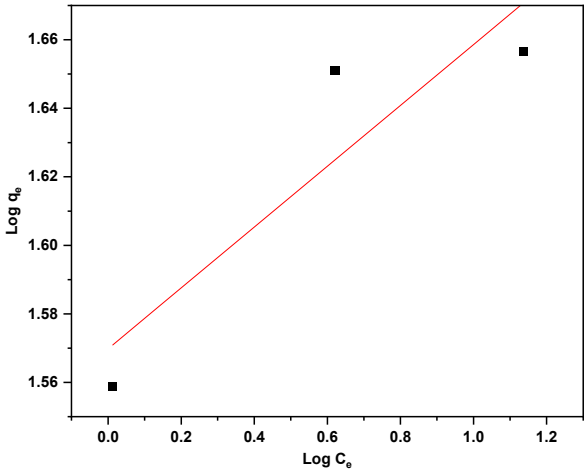

Fig. 18. Freundlich adsorption isotherm of MB dye adsorption by GSANC

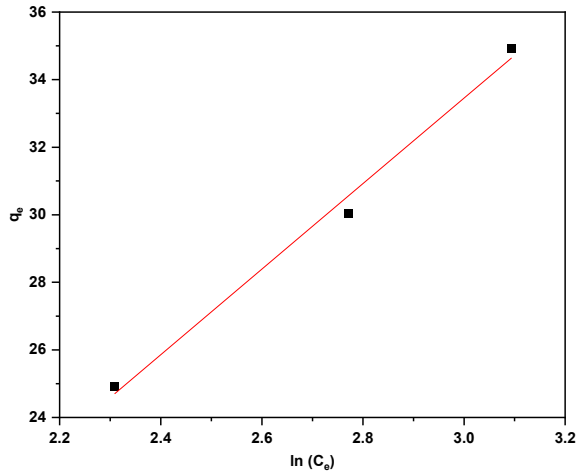

Fig. 19. Temkin adsorption isotherm of MB dye adsorption by GSANC

The adsorption of MB on the GSANC surface followed the Langmuir adsorption isotherm, indicating that the MB uptake occurred as a monolayer on homogenous, fixed adsorption sites. The q_{max} value of 212.76 mg g^{-1} at 30°C demonstrates the adsorption capacity of MB dye ions on GSANC at elevated temperatures. Previously reported ACs properties and q_{max} values are listed in Table 6.

Table 6. q_{max} of MB values of the different ACs and their properties

S.No.	Precursor/Biomass	Activating agent / Chemical	q_{max}	Reference
1.	Groundnut shell	KOH	212.76	This study
2.	Sugarcane bagasse waste	KOH	136.50	(Jawad, Abdulhameed, Bahrudin, et al. 2021)
3.	Dragon fruit peels	KOH	195.20	(Jawad, Abdulhameed, Wilson, et al. 2021)
4.	Bamboo chip	KOH	305.30	(Jawad & Abdulhameed 2020)
5.	Sorghum-Waste	KOH	98.10	(Hou et al. 2020)
6.	Cotton cake	H_3PO_4	333.33	(Ibrahim et al. 2014)
7.	Date pits	$FeCl_3$	259.25	(Theydan & Ahmed 2012)
8.	Groundnut shell	K_2CO_3	210	(Liu et al. 2012)

3.2.1. Adsorption thermodynamics

To determine the thermodynamic functions such as Gibb's free energy (ΔG°) eq. (17, 17a), enthalpy (ΔH°) eq. (19), and entropy (ΔS°) eq. (20), for adsorption of MB dye ions by GSANC:

$$\Delta G° = -RT\ln K \tag{17}$$

$$\text{Whereas } K = \frac{Q_e}{C_e(Q_o - Q_e)} \tag{17a}$$

$$\text{Vant Hoff's equation: } \ln K_d = \frac{\Delta S^o}{R} - \frac{\Delta H^o}{RT} \tag{18}$$

By Vant Hoff's plot (Weber 1995) eq. (18) of lnK versus $\frac{1}{T}$ thermodynamic parameters are determined in, Figure 20. determination of ΔH° and ΔS° Table 7. from the slope and intercept has been done, respectively.

$$\text{Slope} = -\frac{\Delta H^o}{R} \quad \therefore \Delta H° = -(\text{Slope} \times R) \tag{19}$$

$$\text{Intercept} = \frac{\Delta S^o}{R} \quad \therefore \Delta S° = \text{Intercept} \times R \tag{20}$$

where:
K_d – Distribution coefficient,
ΔG° – Gibbs energy,
ΔH° – Enthalpy,
ΔS° – Entropy.

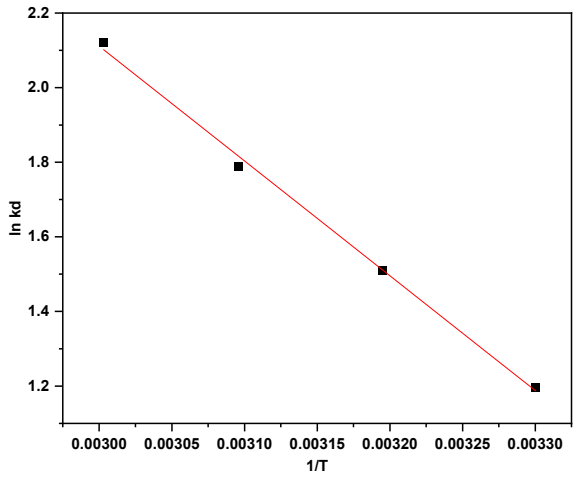

Fig. 20. Vant Hoff's plot (GSANC adsorption of MB dye)

Table 7. Thermodynamic parameters for the adsorption of MB dye on GSANC

Temp (°C)	Temp (K)	K_d	ΔG° (KJ mol^{-1})	ΔH° (KJ mol^{-1})	ΔS° (KJ mol^{-1})
30	303	3.30	-2.98	25.58	0.094
40	313	4.53	-3.93		
50	323	5.98	-4.87		
60	333	8.33	-5.81		

The thermodynamic parameters show that the distribution coefficient (K_d) increases with temperature, indicating improved adsorption capacity of GSANC for Methylene Blue (MB) dye. Negative ΔG° values signify that the adsorption process is spontaneous, whereas positive ΔH° values indicate that the process is endothermic. Positive ΔS° values suggest that MB dye displaces water molecules on GSANC. The increasing K_d values with increasing temperature further highlight the endothermic nature of adsorption process, showing that higher temperatures improve the adsorption of MB dye ions by GSANC.

3.3. Mechanism of MB adsorption on GSANC

GSANC has an excellent porous structure, surface area, and various surface functional groups, enabling efficient MB dye ion removal. Its microporous and mesoporous structure aids dye ion diffusion. As shown in Figure 21, MB ion removal is governed by π-π stacking, electrostatic interactions, and hydrogen bonding. The negatively charged GSANC enhances removal through hydrogen bonding and electrostatic interactions with the cationic dye. Additionally, π-π stacking occurs in between the aromatic rings of the MB dye and the hexagonal structure of GSANC, which contains electron-donating groups like -OH (Guo et al. 2023).

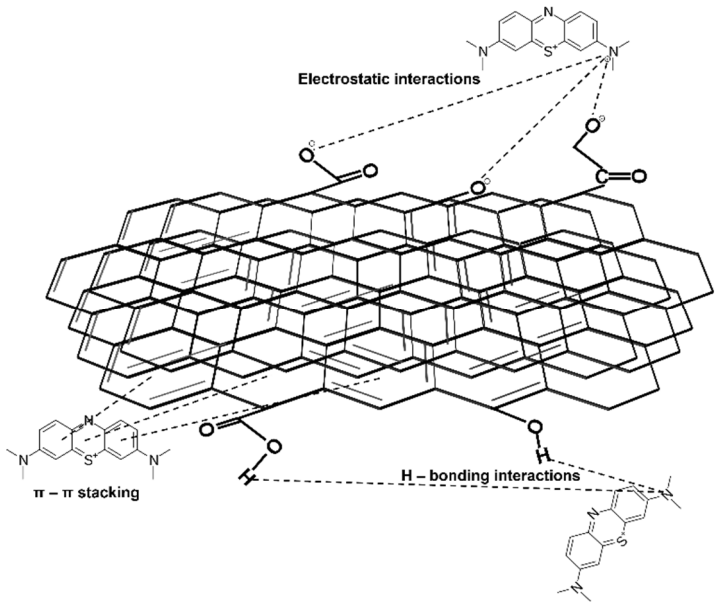

Fig. 21. Schematic illustration of MB dye molecules' interaction with GSANC by electrostatic interactions, π – π stacking and H – bonding interactions

4. Conclusion

In this study, activated carbon derived from groundnut shells was effectively utilized to remove MB dye ions from solutions. This activated carbon underwent various analyses, including FE-SEM with EDS, BET, XRD, FT-IR, TGA, and particle size analysis. The suitable conditions for MB dye adsorption onto the GSANC surface were identified as a dye solution with a pH of 8, an adsorbent dosage of 0.08 g L^{-1}, and a temperature of 303 K. Under these conditions, a maximum Langmuir adsorption capacity (q_{max}) of 212.76 mg g^{-1} was achieved. The adsorption mechanisms involved π-π stacking, hydrogen bonding, and electrostatic interactions. These findings demonstrate that groundnut shell-derived activated carbon is a cost-effective and feasible option for dye adsorption. Additionally, this GSANC is also suitable for the adsorption of pharmaceutical compounds, heavy metals, pesticides, and phenolic compounds.

The authors acknowledge the Department of Environmental Sciences, TNAU, Coimbatore for funding this research under the Sanitation First India Limited Scheme, (Scheme number: F37AMZ).

References

Al-Othman, Z.A., Ali, R., Naushad, M. (2012). Hexavalent chromium removal from aqueous medium by activated carbon prepared from peanut shell: adsorption kinetics, equilibrium and thermodynamic studies. *Chemical engineering journal*, *184*, 238-247. https://doi.org/https://doi.org/10.1016/j.cej.2012.01.048

Benkhaya, S., M'rabet, S., Lgaz, H., El Bachiri, A., El Harfi, A. (2022). Dyes: classification, pollution, and environmental effects. *Dye biodegradation, mechanisms and techniques: Recent advances*, 1-50. https://doi.org/https://doi.org/10.1007/978-981-16-5932-4_1

Bulut, Y., Aydın, H. (2006). A kinetics and thermodynamics study of methylene blue adsorption on wheat shells. *Desalination*, *194*(1-3), 259-267. https://doi.org/https://doi.org/10.1016/j.desal.2005.10.032

EBC, I. (2012). Comparison of European biochar certificate version 4. 8 and IBI biochar standards version 2.0 European Biochar Certificate first publication March 2012b. *www. european-biochar. org/en/home IBI Biochar Stand first Publ May*.

Eldeeb, T.M., Aigbe, U.O., Ukhurebor, K.E., Onyancha, R.B., El-Nemr, M.A., Hassaan, M.A., Ragab, S., Osibote, O.A., El Nemr, A. (2024). Adsorption of methylene blue (MB) dye on ozone, purified and sonicated sawdust biochars. *Biomass Conversion and Biorefinery*, *14*(8), 9361-9383. https://doi.org/https://doi.org/10.1007/s13399-022-03015-w

Georgin, J., Dotto, G L., Mazutti, M.A., Foletto, E.L. (2016). Preparation of activated carbon from peanut shell by conventional pyrolysis and microwave irradiation-pyrolysis to remove organic dyes from aqueous solutions. *Journal of Environmental Chemical Engineering*, *4*(1), 266-275. https://doi.org/https://doi.org/10.1016/j.jece.2015.11.018

Guo, S., Zou, Z., Chen, Y., Long, X., Liu, M., Li, X., Tan, J., Chen, R. (2023). Synergistic effect of hydrogen bonding and π-π interaction for enhanced adsorption of rhodamine B from water using corn straw biochar. *Environmental Pollution*, *320*, 121060. https://doi.org/https://doi.org/10.1016/j.envpol.2023.121060

Hashemi, S.H., Kaykhaii, M. (2022). Azo dyes: sources, occurrence, toxicity, sampling, analysis, and their removal methods. In *Emerging freshwater pollutants* (pp. 267-287). Elsevier. https://doi.org/https://doi.org/10.1016/B978-0-12-822850-0.00013-2

Ho, Y.-S., McKay, G. (1999). Pseudo-second order model for sorption processes. *Process biochemistry*, *34*(5), 451-465.

Hou, J., Liu, Y., Wen, S., Li, W., Liao, R., Wang, L. (2020). Sorghum-waste-derived high-surface area KOH-activated porous carbon for highly efficient methylene blue and Pb (II) removal. *ACS omega*, *5*(23), 13548-13556. https://doi.org/https://doi.org/10.1021/acsomega.9b04452

IBI. (2015). *Specification Standards: Standardized Product Definition and Product Testing Guidelines for Biochar That Is Used in Soil (aka IBI Biochar Standards)* https://biochar-international.org/wp-content/uploads/2023/01/IBI_Biochar_Standards_V2.1_Final.pdf

Ibrahim, T., Moctar, B.L., Tomkouani, K., Gbandi, D.-B., Victor, D.K., Phinthè, N. (2014). Kinetics of the adsorption of anionic and cationic dyes in aqueous solution by low-cost activated carbons prepared from sea cake and cotton cake. *Am. Chem. Sci. J*, *4*(1), 38-57.

Inyang, M., Gao, B., Yao, Y., Xue, Y., Zimmerman, A.R., Pullammanappallil, P., Cao, X. (2012). Removal of heavy metals from aqueous solution by biochars derived from anaerobically digested biomass. *Bioresource technology*, *110*, 50-56. https://doi.org/https://doi.org/10.1016/j.biortech.2012.01.072

Jawad, A.H., Abdulhameed, A.S. (2020). Statistical modeling of methylene blue dye adsorption by high surface area mesoporous activated carbon from bamboo chip using KOH-assisted thermal activation. *Energy, Ecology and Environment*, *5*(6), 456-469. https://doi.org/https://doi.org/10.1007/s40974-020-00177-z

Jawad, A.H., Abdulhameed, A.S., Bahrudin, N.N., Hum, N.N.M.F., Surip, S., Syed-Hassan, S.S.A., Yousif, E., Sabar, S. (2021). Microporous activated carbon developed from KOH activated biomass waste: surface mechanistic study of methylene blue dye adsorption. *Water Science and Technology*, *84*(8), 1858-1872. https://doi.org/https://doi.org/10.2166/wst.2021.355

Jawad, A.H., Abdulhameed, A.S., Wilson, L.D., Syed-Hassan, S.S.A., ALOthman, Z.A., Khan, M.R. (2021). High surface area and mesoporous activated carbon from KOH-activated dragon fruit peels for methylene blue dye adsorption: optimization and mechanism study. *Chinese Journal of Chemical Engineering*, *32*, 281-290. https://doi.org/https://doi.org/10.1016/j.cjche.2020.09.070

Lagergren, S. (1898). About the theory of so-called adsorption of soluble substances.

Langmuir, I. (1916). The constitution and fundamental properties of solids and liquids. Part I. Solids. *Journal of the American chemical society*, *38*(11), 2221-2295. https://doi.org/https://doi.org/10.1021/ja02268a002

Lian, F., Xing, B., Zhu, L. (2011). Comparative study on composition, structure, and adsorption behavior of activated carbons derived from different synthetic waste polymers. *Journal of colloid and interface science*, *360*(2), 725-730. https://doi.org/https://doi.org/10.1016/j.jcis.2011.04.103

Liu, Y., Guo, Y., Gao, W., Wang, Z., Ma, Y., Wang, Z. (2012). Simultaneous preparation of silica and activated carbon from rice husk ash. *Journal of Cleaner Production*, *32*, 204-209. https://doi.org/https://doi.org/10.1016/j.jclepro.2012.03.021

Nam, H., Wang, S., Jeong, H.-R. (2018). TMA and H_2S gas removals using metal loaded on rice husk activated carbon for indoor air purification. *Fuel*, *213*, 186-194. https://doi.org/https://doi.org/10.1016/j.fuel.2017.10.089

Salimi, A., Roosta, A. (2019). Experimental solubility and thermodynamic aspects of methylene blue in different solvents. *Thermochimica Acta*, *675*, 134-139. https://doi.org/https://doi.org/10.1016/j.tca.2019.03.024

Sawalha, H., Bader, A., Sarsour, J., Al-Jabari, M., Rene, E.R. (2022). Removal of dye (methylene blue) from wastewater using bio-char derived from agricultural residues in palestine: Performance and isotherm analysis. *Processes*, *10*(10), 2039. https://doi.org/https://doi.org/10.3390/pr10102039

Sen, T.K. (2023). Adsorptive removal of dye (methylene blue) organic pollutant from water by pine tree leaf biomass adsorbent. *Processes*, *11*(7), 1877. https://doi.org/https://doi.org/10.3390/pr11071877

Senthilkumaar, S., Varadarajan, P., Porkodi, K., Subbhuraam, C. (2005). Adsorption of methylene blue onto jute fiber carbon: kinetics and equilibrium studies. *Journal of colloid and interface science*, *284*(1), 78-82. https://doi.org/https://doi.org/10.1016/j.jcis.2004.09.027

Shan, R., Shi, Y., Gu, J., Wang, Y., Yuan, H. (2020). Single and competitive adsorption affinity of heavy metals toward peanut shell-derived biochar and its mechanisms in aqueous systems. *Chinese Journal of Chemical Engineering*, *28*(5), 1375-1383. https://doi.org/https://doi.org/10.1016/j.cjche.2020.02.012

Sing, K.S. (1985). Reporting physisorption data for gas/solid systems with special reference to the determination of surface area and porosity (Recommendations 1984). *Pure and applied chemistry*, *57*(4), 603-619. https://doi.org/https://doi.org/10.1351/pac198557040603

Supong, A., Bhomick, P.C., Baruah, M., Pongener, C., Sinha, U.B., Sinha, D. (2019). Adsorptive removal of Bisphenol A by biomass activated carbon and insights into the adsorption mechanism through density functional theory calculations. *Sustainable Chemistry and Pharmacy*, *13*, 100159. https://doi.org/https://doi.org/10.1016/j.scp.2019.100159

Temkin, M.J., Pyzhev, V. (1940). Recent modifications to Langmuir isotherms.

Theydan, S.K., Ahmed, M.J. (2012). Adsorption of methylene blue onto biomass-based activated carbon by FeCl3 activation: Equilibrium, kinetics, and thermodynamic studies. *Journal of Analytical and Applied Pyrolysis*, *97*, 116-122. https://doi.org/https://doi.org/10.1016/j.jaap.2012.05.008

Tsade Kara, H., Anshebo, S.T., Sabir, F.K., Adam Workineh, G. (2021). Removal of methylene blue dye from wastewater using periodiated modified nanocellulose. *International Journal of Chemical Engineering*, *2021*(1), 9965452. https://doi.org/https://doi.org/10.1155/2021/9965452

Uchimiya, M., Klasson, K.T., Wartelle, L.H., Lima, I.M. (2011). Influence of soil properties on heavy metal sequestration by biochar amendment: 1. Copper sorption isotherms and the release of cations. *Chemosphere*, *82*(10), 1431-1437. https://doi.org/https://doi.org/10.1016/j.chemosphere.2010.11.050

Wang, B., Qiu, J., Feng, H., Sakai, E., Komiyama, T. (2016). KOH-activated nitrogen doped porous carbon nanowires with superior performance in supercapacitors. *Electrochimica Acta*, *190*, 229-239. https://doi.org/https://doi.org/10.1016/j.electacta.2016.01.038

Weber, G. (1995). van't Hoff revisited: enthalpy of association of protein subunits. *The Journal of Physical Chemistry*, *99*(3), 1052-1059. https://doi.org/https://doi.org/10.1021/j100003a031

Xing, S., Hu, C., Qu, J., He, H., Yang, M. (2008). Characterization and reactivity of MnO x supported on mesoporous zirconia for herbicide 2, 4-D mineralization with ozone. *Environmental science & technology*, *42*(9), 3363-3368. https://doi.org/https://doi.org/10.1021/es0718671

Xu, Z., Chen, J., Zhang, X., Song, Q., Wu, J., Ding, L., Zhang, C., Zhu, H., Cui, H. (2019). Template-free preparation of nitrogen-doped activated carbon with porous architecture for high-performance supercapacitors. *Microporous and Mesoporous Materials*, *276*, 280-291. https://doi.org/https://doi.org/10.1016/j.micromeso.2018.09.023

Zhou, Y., Zhang, L., Cheng, Z. (2015). Removal of organic pollutants from aqueous solution using agricultural wastes: a review. *Journal of Molecular Liquids*, *212*, 739-762. https://doi.org/https://doi.org/10.1016/j.molliq.2015.10.023